NMR and Computational Characterization of the *N*-(Deoxyguanosin-8-yl)aminofluorene Adduct [(AF)G] opposite Adenosine in DNA: (AF)G[syn]·A[anti] Pair Formation and Its pH Dependence†

David Norman,‡ Perlet Abuaf,‡ Brian E. Hingerty,§ David Live,∥ Dezider Grunberger,‡ Suse Broyde,⊥ and Dinshaw J. Patel*,‡

Department of Biochemistry and Molecular Biophysics, College of Physicians and Surgeons, Columbia University, New York, New York 10032, Health and Safety Research Division, Oak Ridge National Laboratory, Oak Ridge, Tennessee 37831, Chemistry Department, Emory University, Atlanta, Georgia 30322, and Biology Deparment, New York University, New York, New York 10003

Received March 8, 1989; Revised Manuscript Received May 25, 1989

ABSTRACT: This paper reports on a combined two-dimensional NMR and energy minimization computational characterization of the conformation of the *N*-(deoxyguanosyl-8-yl)aminofluorene adduct [(AF)G] positioned across adenosine in a DNA oligomer duplex as a function of pH in aqueous solution. This study was undertaken on the d[C1-C2-A3-T4-C5-(AF)G6-C7-T8-A9-C10-C11]·[G12-G13-T14-A15-G16-A17-G18-A19-T20-G21-G22] complementary undecamer [(AF)G 11-mer duplex]. The modification of the single G6 on the pyrimidine-rich strand was accomplished by reaction of the oligonucleotide with *N*-acetoxy-2-(acetylamino)fluorene and subsequent deacetylation under alkaline conditions. The HPLC-purified modified strand was annealed with the unmodified purine-rich strand to generate the (AF)G 11-mer duplex. The exchangeable and nonexchangeable protons are well resolved and narrow in the NMR spectra of the (AF)G 11-mer duplex so that the base and the majority of sugar nucleic acid protons, as well as several aminofluorene ring protons, have been assigned following analysis of two-dimensional NOESY and COSY data sets at pH 6.9, 30 °C in H_2O and D_2O solution. The NOE distance constraints establish that the glycosidic torsion angle is syn at (AF)G6 and anti at A17, which results in the aminofluorene ring being positioned in the minor groove. A very large downfield shift is detected at the H2′ sugar proton of (AF)G6 associated with the (AF)G6[syn]·A17[anti] alignment in the (AF)G 11-mer duplex. The NMR parameters demonstrate formation of Watson–Crick C5·G18 and C7·G16 base pairs on either side of the (AF)G6[syn]·A17[anti] modification site with the imino proton of G18 more stable to exchange than the imino proton of G16. Several nonexchangeable aminofluorene protons undergo large downfield shifts as do the imino and H8 protons of G16 on lowering of the pH from neutrality to acidic values for the (AF)G 11-mer duplex. Both the neutral and acidic pH conformations have been defined by assigning the NOE constraints in the [C5-(AF)G6-C7]·[G16-A17-G18] segment centered about the modification site and incorporating them in distance constrained minimized potential energy calculations in torsion angle space with the DUPLEX program. A series of NOEs between the aminofluorene protons and the DNA sugar protons in the neutral pH conformation establish that the aminofluorene ring spans the minor groove and is directed toward the G16-A17-G18 sugar–phosphate backbone on the partner strand. An unconstrained minimum energy neutral pH conformation for the (AF)G 11-mer duplex was generated from the minimization runs which satisfies the NMR distance constraints and is stabilized by hydrophobic interactions between the aminofluorene ring and the walls of the minor groove. The backbone of A17 adopts a B_{II} conformation (ϵ, ζ = g^-, t) and the sugar ring of G16 adopts a C3′-endo pucker which facilitates, in part, a small displacement of A17 toward the major groove and minimizes the total solvent exposure of aminofluorene and A17 at the modification site. There is poor stacking between bases in the C5-(AF)G6-C7 segment but strong stacking between bases in the G16-A17-G18 segment consistent with the large upfield shifts of the H8 protons of G16 and G18 in the (AF)G 11-mer duplex. The NOE constraints establish that the (AF)G6[syn]·A17[anti] alignment is retained on lowering of the pH but is accompanied by the loss of contacts between the aminofluorene ring of (AF)G6 and the G16-A17-G18 sugar–phosphate backbone on the partner strand. A minimum energy acidic pH conformation is proposed for the [C5-(AF)G6-C7]·[G16-A17-G18] segment involving protonated (AF)G6[syn]·A17[anti] pairing stabilized by one hydrogen bond between the N1 of protonated A17 and the O6 of (AF)G6. This alignment results in the displacement of the aminofluorene ring away from the helix axis in the minor groove. Our studies establish an interplay between hydrophobic and hydrogen-bonding contributions to the stabilization of the (AF)G6[syn]·A17[anti] modification site.

The carcinogen *N*-acetoxy-2-(acetylamino)fluorene (AAAF) binds with high specificity to the C8 position of guanosine in DNA [reviewed in Singer and Grunberger (1983)]. This *N*-(deoxyguanosin-8-yl)-2-(acetylamino)fluorene adduct [(AAAF)G] is deacetylated by cellular enzymes to the *N*-(de-

† This research was supported by NIH CA-21111 (D.J.P. and D.G.), by NIH CA-28038, DOE Contract DE-AC02-91ER60015, and NSF DMB-8416009 (S.B.), by DOE Contract DE-AC05-840R21400 with Martin-Marietta Energy Systems (B.E.H.), and by NSF DMB-8604304 (D.L.). S.B. thanks DOE for a Grand Challenge Award for computer time.

‡ Columbia University.
§ Oak Ridge National Laboratory.
∥ Emory University.
⊥ New York University.

0006-2960/89/0428-7462$01.50/0

oxyguanosin-8-yl)aminofluorene adduct [(AF)G], which is the major and most persistent adduct in mammalian systems (Irving, 1966; Kriek, 1969; Irving & Veazey, 1969; Beland et al., 1982; Poirier et al., 1982).

There is extensive literature on molecular models of (AAF)G and (AF)G incorporated into both right-handed and left-handed DNA (Evans et al., 1980; Broyde & Hingerty, 1983, 1987; Neidle et al., 1984; Hingerty & Broyde, 1982, 1986). These modeling studies supported the view, suggested from experimental studies (Singer & Grunberger, 1983), that the *anti*-guanosine C8 position, being directed toward the phosphodiester backbone in right-handed B-DNA, cannot accommodate a bulky AAF substituent. The *syn*-guanosine C8 position, on the other hand, is directed toward solvent in left-handed Z-DNA and can readily accomodate a bulky AAF substituent. The base displacement (Grunberger et al., 1970) and insertion–denaturation (Fuchs & Daune, 1972) models for right-handed (AAF)G-modified DNA orient the *syn*-guanosine so that it is displaced from the helix by the attached AAF chromophore which stacks with adjacent base pairs.

Earlier experimental studies suggested less distortion to the B-DNA duplex by AF adducts than by AAF adducts (Sage et al., 1979; Kriek & Spelt, 1979; Santella et al., 1980; Rio et al., 1980; Leng et al., 1980; Evans et al., 1980) and have been interpreted to imply that the AF can reside in the major groove of an undistorted B-DNA duplex (Evans et al., 1980). Recent spectroscopic studies have been interpreted to support a base displacement model for the AF adduct (van Houte et al., 1987a,b). Previous potential energy calculations for the AF adduct in a deoxynucleoside (Lipkowitz et al., 1982), deoxydinucleoside monophosphate (Broyde & Hingerty, 1983), and larger structures (Hingerty & Broyde, 1986) were restricted to alternating C-G sequences in single strands and in duplexes with standard Watson–Crick base pairs. These studies indicated a heterogeneity of conformational possibilities for the AF adduct: *syn*- and *anti*-guanosines, as well as base–base-stacked and carcinogen–base-stacked states, are energetically feasible when the acetyl is absent.

The selective incorporation of (AAF)G into oligonucleotide duplexes has been accomplished through chemical modification of a single guanosine in a DNA oligomer strand by treatment with *N*-acetoxy-2-(acetylamino)fluorene (Sharma & Box, 1985; Sanford & Krugh, 1985). The selective incorporation of (AF)G into oligonucleotide duplexes has been accomplished either through direct synthesis (Stohrer et al., 1980; O'Connor & Stohrer, 1985; Mitchell & Stohrer, 1986) or by chemical modification of a single guanosine in a DNA oligomer strand with *N*-acetoxy-*N*-(trifluoroacetyl)-2-aminofluorene (Johnson et al., 1986; Michaels et al., 1987). The lesion-containing strand can then be paired to the complementary strand to generate duplexes containing either a single (AAF)G or a single (AF)G site.

High-resolution proton NMR methods have been applied to elucidate structural features of AAF–G adducts at the mononucleotide (Evans & Levine, 1987), dinucleotide (Evans & Levine, 1988), and hexanucleotide (Sharma & Box, 1985) single-strand level and at the nonanucleotide duplex level (Krugh et al., 1986). The latter NMR study addresses questions related to the conformation of (AAF)G opposite cytidine in the center of a 9-mer duplex (Krugh et al., 1986). Further details of this structure will be of great interest.

The NMR studies reported in this paper focus on the major persistent (AF)G adduct embedded at a single site in a DNA oligomer duplex. The recent review by Basu and Essigmann (1988) brought to our attention an earlier report that AF-induced mutations are predominantly G·C → T·A transversions (Bichara & Fuchs, 1985), and so, our approach focused on NMR studies of a DNA oligomer containing an (AF)G lesion opposite an adenosine in the center of the duplex.

We report below on a two-dimensional NMR study of the complementary d[C-C-A-T-C-(AF)G-C-T-A-C-C]·d[G-G-T-A-G-A-G-A-T-G-G] duplex [designated (AF)G 11-mer duplex, **1**] at neutral and acidic pH in H_2O and D_2O solution. The experimental NMR distance constraints are combined with energy minimization calculations to define the neutral pH and acidic pH conformations centered about the (AF)G·A lesion site in the (AF)G 11-mer duplex.

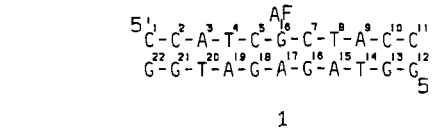

1

Experimental Procedures

Oligonucleotide Synthesis. The oligonucleotides d(C-C-A-T-C-G-C-T-A-C-C) and d(G-G-T-A-G-A-G-A-T-G-G) were synthesized on a Beckman System 1+ automated DNA synthesizer using a solid-phase cyanoethyl phosphoramidite approach. The crude, 5′-dimethoxytritylated oligonucleotides were isolated by treatment of the support with concentrated aqueous ammonia for 36 h at room temperature. Purification of the products was by reverse-phase HPLC in two stages followed by desalting on Sephadex G-25. The oligomers were finally converted to sodium form by passage through a short column of Dowex 50X8 cation exchange resin.

Preparation of Aminofluorene Adduct. Samples of the oligonucleotide d[C-C-A-T-C-G-C-T-A-C-C] were converted into the aminofluorene adduct d[C-C-A-T-C-(AF)G-C-T-A-C-C] in two steps. The oligonucleotide was first converted into its (acetylamino)fluorene adduct by treating the oligomer, dissolved in 0.002 M sodium citrate buffer, pH 7.1, with an excess of *N*-acetoxy-2-(acetylamino)fluorene, dissolved in absolute ethanol (10 mg/mL), in a molar ratio of 1:8. The mixture was shaken at 37 °C in the dark for 3 h and then extracted with water-saturated diethyl ether. The crude AAF-modified oligomer contained in the remaining aqueous solution was purified by C3 reverse-phase HPLC using a linear gradient of acetonitrile against 0.01 M triethylammonium acetate buffer, pH 7.1 (0–25% in 30 min).

The pure AAF-modified oligomer was converted into the AF-modified oligomer by dissolution in 1 M NaOH containing 0.3% (v/v) 2-mercaptoethanol at a concentration of 2 mg/mL. The reaction was allowed to proceed for 45 min at room temperature and then neutralized with dilute hydrochloric acid. After extensive purging of the solution with nitrogen and desalting on a Sephadex G-25 column, the AF-modified oligomer was purified by HPLC as in the case of the AAF-modified oligomer.

The pure AF-modified oligomer was desalted on Sephadex G-25 and converted to sodium form on Dowex 50X8 cation exchange resin.

The ratio (A_{260} absorption units) of the AF adduct containing strand to its partner strand was determined by preparing samples of both strands in buffered D_2O solutions (0.4 mL) and titrating the AF adduct containing strand with its partner strand as followed by one-dimensional NMR at elevated temperature. A 1:1 molar ratio of the AF adduct containing strand to the partner strand was achieved following addition of 49 A_{260} to 51 A_{260} of the corresponding sequences. This approach was used to prepare the duplex on a 500 OD A_{260} unit scale.

Sample Preparation. The NMR spectra of the parent and the AF adduct duplexes were recorded in 0.1 M NaCl–10 mM phosphate–1 mM EDTA solutions of either 99.96% D_2O or 90% H_2O/10% D_2O (v/v). The pH values of the samples were as described under Results, and the concentration was 500 A_{260} units/0.4 mL of solution.

Proton NMR Studies. One- and two-dimensional proton NMR data sets were recorded on Bruker AM 400 and AM 500 spectrometers. Proton chemical shifts were referenced relative to internal 3-(trimethylsilyl)propionate-*2,2,3,3-d*$_4$ (TSP). Phase-sensitive two-dimensional proton NOESY spectra in H_2O buffer were collected by quadrature detection with a 120-ms mixing time. The carrier frequency was placed directly on the H_2O signal, and an optimized jump–return pulse scheme giving even excitation of imino, amino, and aromatic protons was used. The time domain data sets consisted of 1024 complex data points over a sweep width of 8064 Hz collected over 512 t_1 experiments with a 1.0-s repetition delay and 256 scans per increment. The real and imaginary data sets were collected sequentially and merged to yield 256 complex t_1 increments. The free induction decays were apodized with a 90°-shifted sine bell function to remove truncation effects, and 3-Hz line broadening was applied in both dimensions, to improve signal to noise. A fifth-order polynomial base-line correction was applied in both dimensions.

Phase-sensitive two-dimensional proton NOESY spectra in D_2O were collected with a 2.0-s repetition time, a sweep width of 4000 Hz, and mixing times of either 250 or 300 ms. The carrier frequency was placed on the residual HOD resonance, which was irradiated with the decoupler channel. The data sets were collected with 512 t_1 experiments using 1024 complex data points in the t_2 dimension and 32 scans per t_1 increment. Real and imaginary data points were acquired sequentially and then merged to yield 256 complex t_1 points. The data sets were apodized with a 90° sine bell function, and 3-Hz line broadening was used in both dimensions. Spectra were symmetrized.

Magnitude two-dimensional proton correlated (COSY) experiments were recorded with quadrature detection in both dimensions. The data sets were collected with 512 t_1 increments and a sweep width of 4000 Hz with 1024 complex data points in the t_2 dimension. A repetition delay of 1.0 s and 32 scans per t_1 increment were used. The data sets were apodized with an unshifted sine bell function zeroed to the 512th point and Fourier transformed in both dimensions.

Phase-sensitive two-dimensional proton HOHAHA spectra were recorded with a spin lock time of 51 ms. The data sets were collected with 512 t_1 experiments using 1024 complex data points in the t_2 dimension and 128 scans per t_1 increment. Real and imaginary data points were acquired sequentially and then merged to yield 256 complex t_1 points. The data were apodized with a 90°-shifted sine bell function and base line corrected with a fifth-order polynomial in both dimensions.

Phase-sensitive two-dimensional proton double quantum-filtered (DQF) COSY spectra were obtained with a sweep width of 4000 Hz; 2048 data points in the t_2 dimension and 356 t_1 increments were collected; a repetition delay of 1 s was used and 64 scans per t_1 increment.

Phosphorus NMR Studies. Phase-sensitive two-dimensional proton-detected proton–phosphorus COSY spectra were recorded with 5-mm proton reverse detection and a broad-band decoupler accessory on the GN 500 spectrometer. The pulse sequence in the heteronuclear two-dimensional experiments was as described previously (Sklenar et al., 1986) except for the receiver phase cycling which should be corrected to sequence B in Sklenar and Bax (1987). A string of 34 (n = 34) 180° pulses separated by a d value of 50 ms were used in the beginning of the sequence to saturate the protons, and a postacquisition delay of 100 ms was used before restarting the sequence. Alternate acquisitions were checked in alternate memory blocks and were processed to give phase-sensitive two-dimensional spectra (States et al., 1982). For the two-dimensional data set, 256 scans were collected for each of 128 t_1 values used. Spectral width in the proton dimension was 2000 Hz in 1024 points, and the width in the phosphorus dimension was 1000 Hz in 128 points. The phosphorus dimension was zero filled twice in processing. The DM apodization function in the GN software was used with a value of 3 in both dimensions. Data were processed on the Nicolet 1280 computer on the spectrometer. Chemical shifts were referenced to trimethyl phosphate (TMP) in D_2O indirectly based on a measurement of a sample of TMP and TSP in D_2O and following the procedure for relating proton standard positions to that of another nucleus described elsewhere (Live et al., 1984).

Computational Studies. Minimized potential energy calculations in torsion angle space were carried out with the program DUPLEX which has recently been described in full detail (Hingerty & Broyde, 1986; Broyde & Hingerty, 1987), with complete parametrizations (Hingerty et al., 1989). The potential set is similar to one devised by Srinivasan and Olson (1980). It includes van der Waals, electrostatic, torsional, deoxyribose strain, and anomeric gauche terms. In addition, counterion condensation and solvent are mimicked by employing reduced partial charges on the nonlinked phosphate oxygens and a distance-dependent dielectric constant, respectively.

For duplexes, a hydrogen-bond potential similar to that of Olson (1978) is employed. A standard 6-12 Lennard–Jones potential is applied to selected atoms involved in a hydrogen bond, but the Lennard–Jones parameters are altered to permit the appropriate closer approach. This treatment yields hydrogen-bonded structures from minimizations of conformers whose starting conformation is close to hydrogen bonded and low energy. However, because of the multiple minimum problem, hydrogen-bonded structures may not be found from high-energy starting conformations. To overcome this problem, minimizations are carried out in stages. In the first stage a mathematical forcing function, F, added to the energy is employed to *locate* hydrogen-bonded minimum energy conformations. This pseudopotential function, with units of energy in kcal/mol, is non-negative and equals zero when an ideal hydrogen bond is formed:

$$F_{HB} = W_{HB}\sum_{1}^{n}\{(d - d_0)^2 + (1 + \cos[\tau])^2 + p\} \quad (1)$$

The instantaneous value of the hydrogen-bond distance is d, d_0 is its ideal value, τ is the instantaneous value of the angle about the hydrogen participating in the hydrogen bond (its ideal value is 180°) and $p = |\mathbf{c}_1 - \mathbf{c}_2|^2$, where $\mathbf{c}_1$ is a unit vector perpendicular to the plane of one base and $\mathbf{c}_2$ is a unit vector perpendicular to the plane of its partner. The ideal values, d_0, are taken from Arnott et al. (1976) for Watson–Crick base pairs and are 2.93, 2.86, and 2.90 Å for N1A-N7G, N6A-O6G, and N1A-O6G, respectively (see below). $\mathbf{c}_2$ is parallel to $\mathbf{c}_1$ when the ideal hydrogen bond is formed. W_{HB} is an adjustable weight and was usually assigned a value of 7.5 in the duplex trimer trials and 30 in larger structures. F is summed over all n hydrogen bonds. A first minimization is carried out with the function F_{HB} implemented for the selected hydrogen-bonding partners.

To locate minimum energy conformations with interatomic

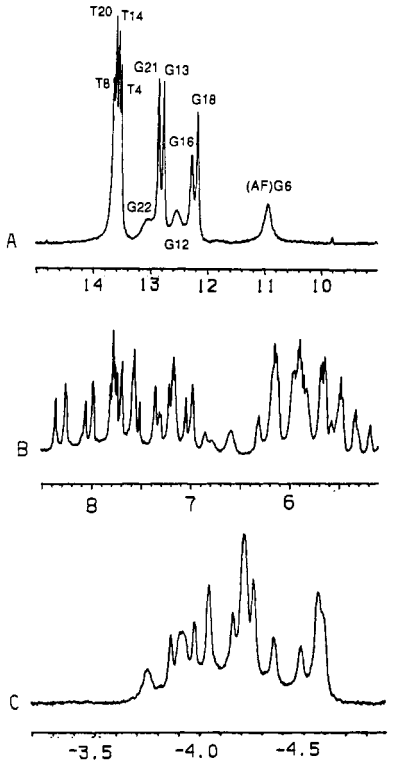

FIGURE 1: (A) Proton NMR spectrum (9.0–15.0 ppm) of the (AF)G 11-mer duplex in H_2O–buffer, pH 6.9 at 20 °C. (B) Proton NMR spectrum (5.0–8.5 ppm) of the (AF)G 11-mer duplex in D_2O–buffer, pH 6.93 at 30 °C. (C) Proton-decoupled phosphorus NMR spectrum of the (AF)G 11-mer duplex in D_2O–buffer, pH 6.9 at 30 °C. The buffer was 0.1 M NaCl–10 mM phosphate–aqueous solution.

distances suggested from experimental NMR data, treatments analogous to the one used to locate particular hydrogen-bonding schemes are employed. A pseudopotential (of no thermodynamic significance) with energies in kcal/mol is again added to the energy. For the n NOE measured distances

$$F_N = W_N \sum_1^n (d - d_N)^2 \quad (2)$$

where W_N is the adjustable weight, d is the instantaneous value of the distance, and d_N is its target value. This term is implemented only for d greater than d_N. For d less than d_N, F_N is assigned a value of zero. Thus, any distance between d_N and the sum of the van der Waals radii plus 0.2 Å (as required by our parametrization of the Lennard–Jones potential) is accepted. For constraints of distances within narrow ranges the pseudopotential term used is

$$F_S = W_S \sum_1^n (d - d_S)/\Delta^2 \quad (3)$$

where W_S is the adjustable weight, d and d_s are instantaneous and target distances, and Δ is a selected tolerance factor for the distance. In the present work, W_N was assigned values in the range of 1–12 for trimers and 3–20 for larger structures. Δ values are in the range of 0.01–0.05. W_S was assigned a value of 9, which allows a maximum tolerance of three standard deviations.

In the final minimization stages all constraints (F_{HB}, F_N, and F_S) are released in the neutral pH structure for which a full data set was on hand, producing a structure that is an unconstrained energy minimum that matches the NMR data. Thus, the constraints are a strategy for dealing with the multiple minimum problem, that is, for *locating* minimum energy conformations consistent with the NMR data.

The two strands of the duplex were positioned so that the first base pair was oriented exactly as in the B-DNA fiber diffraction model (Arnott et al., 1976). Bond lengths and bond angles for N1-protonated adenosine were taken from the structure of UpA+ (Rubin et al., 1976). Partial charges for N1-protonated 9-methyladenine were kindly supplied by Dr. Rick Ornstein and are consistent with the rest of our charge set for DNA, computed by Ornstein and Rein (1976). The protonated adenine charges are given in Table A (see supplementary material).

Parametrization for AF and linkage site is the same as detailed in previous work (Broyde & Hingerty, 1983). The (AF)G linkage torsion angles are defined as follows: α', N9(G)–C8(G)–N(AF)–C2(AF); β', C8(G)–N(AF)–C2(AF)–C1(AF). The DNA torsion angles are as follows: χ(pyr), O1′–C1′–N1–C2; χ(pur), O1′–C1′–N9–C4; ϵ, P–O3′–C3′–C4′; ζ, O5′–P–O3′–C3′; α, C5′–O5′–P–O3′; β, C4′–C5′–O5′–P; γ, C3′–C4′–C5′–O5′. The angle A–B–C–D is measured by a clockwise rotation of D with respect to A, looking down the B–C bond. A eclipsing D is 0°. Sugar pucker is determined by the pseudorotation parameter **P** (Altona & Sundaralingam, 1972).

The search strategies employed to define the structure of the AF-modified 11-mer duplex are given under Results.

Results

(1) NMR Assignments and Constraints for (AF)G 11-mer at Neutral pH

The initial efforts have focused on two-dimensional NMR studies of the (AF)G 11-mer at neutral pH with the emphasis on spectral assignments and the identification of distance-dependent NOE constraints centered about the covalent modification site.

Exchangeable Nucleic Acid Protons. The proton spectra (5.5–14 ppm) of the (AF)G 11-mer duplex in H_2O buffer, pH 6.9 at 20 °C, is plotted in Figure 1A. Eleven partially resolvable exchangeable protons are detected between 10.5 and 14.0 ppm with several broad resonances in the 20 °C spectrum. The imino proton at ~11.0 ppm is upfield shifted from the remaining imino protons which resonate between 12.0 and 14.0 ppm (Figure 1A).

The imino protons have been assigned from an analysis of the NOESY (125-ms mixing time) spectrum of the (AF)G 11-mer duplex in H_2O buffer, pH 6.9 at 5 °C. The expanded NOESY contour plot establishing distance connectivities in the symmetrical 10.8–14.0 ppm region are plotted in Figure 2A, that between the 10.8–14.0 ppm and the 4.8–8.6 ppm region is plotted in Figure 2B, and that between the 6.4–8.8 ppm and the 4.8–7.6 ppm region is plotted in Figure A (supplementary material). The four thymidine imino protons (13.5–13.75 ppm) exhibit NOEs to the adenosine H2 protons within individual A·T pairs (peaks E, F, G, and H, Figure 2B) while the nonterminal guanosine imino protons (12.1–13.2 ppm) exhibit NOEs to hydrogen-bonded and exposed cytidine amino protons within individual G·C pairs (peaks J and I, L and K, O and M, and R and P, Figure 2B). The imino protons at 13.11 and 12.72 ppm are assigned to the terminal G·C pairs since these protons broaden to the greatest extent on raising of the temperature and because they exhibit strong crosspeaks to the H_2O resonance (peaks U and V, Figure 2B).

The guanosine imino protons in the (AF)G 11-mer duplex are assigned by monitoring their NOEs to the hydrogen-bonded and exposed cytidine amino protons across the G·C pair which in turn exhibit NOEs to the H5 protons within the cytidine ring. The cytidine H5 assignments can be rigorously

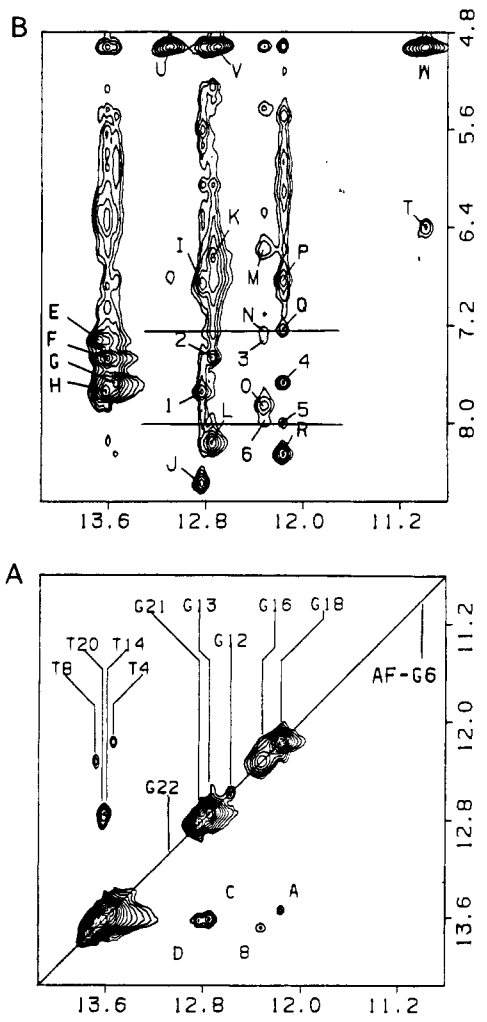

FIGURE 2: Phase-sensitive NOESY (mixing time 125 ms) contour plots of the (AF)G 11-mer duplex in 0.1 M NaCl–10 mM phosphate–H_2O, pH 6.9 at 5 °C. (A) Crosspeaks establishing distance connectivities in the symmetrical 10.8–14.0 ppm imino proton range. (B) Crosspeaks establishing distance connectivities between the imino protons (10.8–14.0 ppm) and the base and amino protons (4.8–8.6 ppm). The crosspeaks assignments are discussed in the text.

established from an analysis of the NOESY spectra of the (AF)G 11-mer duplex recorded in D_2O solution. The crosspeaks between the hydrogen-bonded and exposed amino protons of cytidine are designated CN, between the hydrogen-bonded amino and H5 protons of cytidine by CN5, and between the H6 and H5 protons of cytidine by C* for cytidines C1, C2, C5, C7, C10, and C11 in the (AF)G 11-mer duplex in Figure A (supplementary material). The guanosine imino and cytidine amino proton assignments in the (AF)G 11-mer duplex are listed in Table I.

The assigned guanosine imino protons of G·C pairs can then be correlated on the basis of observed NOEs to the thymidine imino (Figure 2A) and adenosine H2 (Figure 2B) of adjacent A·T pairs in the (AF)G 11-mer duplex. Thus, NOEs are detected between adjacent C2·G21 and A3·T20 pairs (peak D, Figure 2A; peak 1, Figure 2B), between adjacent T4·A19 and C5·G18 pairs (peak A, Figure 2A; peak 4, Figure 2B), between adjacent C7·G16 and T8·A15 pairs (peak B, Figure 2A; peak 3, Figure 2B), and between adjacent A9·T14 and C10·G13 pairs (peak C, Figure 2A; peak 2, Figure 2B). The thymidine imino and adenosine H2 proton assignments in the (AF)G 11-mer duplex are listed in Table I.

The remaining guanosine imino proton at 10.98 ppm is assigned to (AF)G6 and exhibits an NOE to its own amino

Table I: Exchangeable Proton Chemical Shifts in the (AF)G 11-mer in 0.1 M NaCl–10 mM Phosphate–H_2O, pH 6.9, 5 °C

	chemical shifts (ppm)				
base pair	G-N1H	T-N3H	C-N4Hb	C-N4He	A-H2
C1·G22	13.11		7.95	6.83	
C2·G21	12.85		8.52	6.90	
A3·T20		13.64			7.76
T4·A19		13.56			7.69
C5·G18	12.18			6.86	
(AF)G6·A17	10.98				8.02
C7·G16	12.34		7.88	6.61	
T8·A15		13.69			7.35
A9·T14		13.62			7.49
C10·G13	12.76		8.18	6.68	
C11·G12	12.72		8.16	6.85	

protons at 6.4 ppm (peak T, Figure 2B) and a strong NOE to the H_2O resonance (peak W, Figure 2B). The latter observation suggests that the guanosine imino proton of (AF)G6 is accessible to solvent in the (AF)G 11-mer duplex.

The imino protons of C5·G18 and C7·G16 which flank the (AF)G6·A17 lesion site exhibit weak NOEs to the adenosine H2 proton of A17 (peaks 5 and 6, Figure 2B) and the H1 proton of the AF ring (peaks Q and N, Figure 2B) in the (AF)G 11-mer duplex. These NOEs provide important constraints in defining the conformation of the three base pair segment centered about the (AF)G6·A17 lesion site.

The temperature dependence of the imino proton line widths in the (AF)G 11-mer duplex in Figure 1A establishes that the imino protons of the terminal C1·G22 and C11·G12 base pairs are most labile followed by those of the (AF)G6·A17 lesion site. Further, line-width differences are detected for the imino protons of C7·G16 and C5·G18 which flank the lesion site with the imino proton of G16 broader than that of G18 in the (AF)G 11-mer duplex (Figure 1A).

Exchangeable Aminofluorene Protons. There is a single NH proton on the aminofluorene ring which is linked to the C8 position of G6. All of the exchangeable protons downfield of 8.5 ppm are accounted for, and hence, this proton must resonate upfield of 8.5 ppm. We have been unable to locate this aminofluorene exchangeable proton in the spectrum of the (AF)G 11-mer duplex at this time.

Nonexchangeable Nucleic Acid Protons. The nonexchangeable proton spectra (5.0–8.5 ppm) of the (AF)G 11-mer duplex in D_2O buffer, pH 6.93 at 30 °C, is plotted in Figure 1B. The nonexchangeable base and sugar H1′ protons are partially resolved in this region and can be investigated further by recording two-dimensional NOESY and COSY data sets. The phase-sensitive NOESY spectrum (300-ms mixing time) of the (AF)G 11-mer duplex in D_2O buffer, pH 6.9 at 30 °C, exhibits resolved crosspeaks so that the NOE distance connectivities can be systematically assigned to yield the nucleic acid base and a majority of the sugar proton assignments, as well as several aminofluorene assignments.

The expanded NOESY plots establishing distance connectivities between the base protons (6.9–8.4 ppm) and the sugar H1′ and cytidine H5 protons (5.1–6.4 ppm) in the (AF)G 11-mer duplex are plotted in duplicate in Figure 3. Each base proton (purine H8/pyrimidine H6) exhibits two NOE crosspeaks to sugar H1′ protons, one of which is to its own and the other to the 5′-linked sugar H1′ proton on the same strand in the helix (Hare et al., 1983). This permits the chain to be traced from C1 to C5 and from C7 to C11 in the modified strand (Figure 3A) and from G12 to G22 in the unmodified strand (Figure 3B) of the (AF)G 11-mer duplex. The interruption in the tracing at (AF)G6 on the modified strand is due to the absence of a purine H8 proton as a result of the

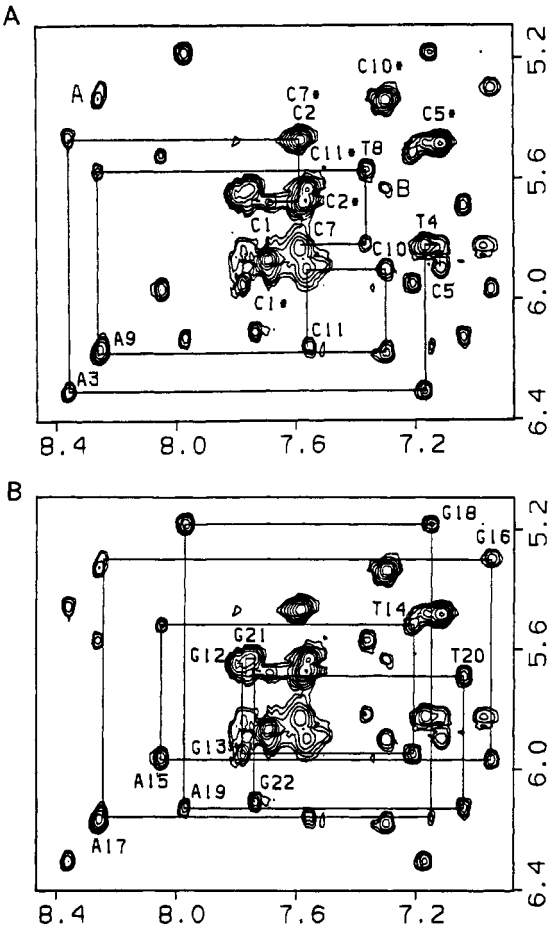

FIGURE 3: Phase-sensitive expanded NOESY contour plots (mixing time 300 ms) of the (AF)G 11-mer duplex in 0.1 M NaCl–10 mM phosphate–D_2O, pH 6.9 at 30 °C, establishing distance connectivities between the base protons (6.8–8.4 ppm) and the sugar H1′ and cytidine H5 protons (5.0–6.4 ppm). The chain is traced from C1 to C11 in (A), and the chain is traced from G11 to G22 in (B). The tracing follows connectivities between adjacent base protons through their intervening sugar H1′ protons. The cytidine H5–H6 connectivities are designated by asterisks.

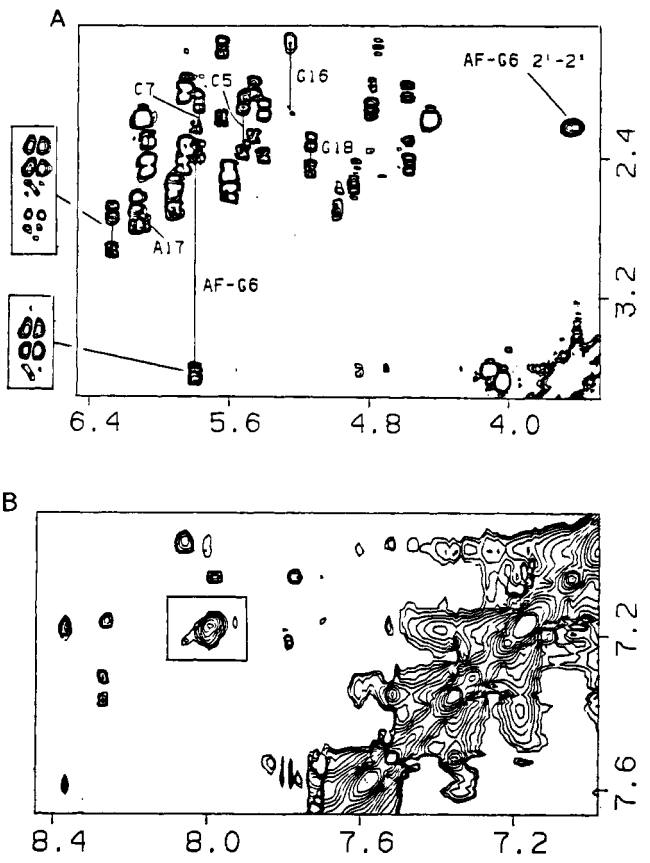

FIGURE 4: (A) Expanded magnitude COSY contour plot of the (AF)G 11-mer duplex in 0.1 M NaCl–10 mM phosphate–D_2O, pH 6.9 at 30 °C, establishing coupling connectivities between the H1′ and H3′ protons (3.6–6.4 ppm) and the H2′,2″ protons (1.6–3.8 ppm). The magnitude data set was supplemented by a phase-sensitive DQF-COSY data set on the (AF)G 11-mer duplex. Typical crosspeaks in the DQF-COSY experiment are presented as boxed expansions to the left of the figure. (B) Expanded phase-sensitive NOESY (mixing time 300 ms) establishing distance connectivities between the 7.0–8.4 ppm and the 7.0–7.6 ppm regions of the (AF)G 11-mer duplex in 0.1 M NaCl–10 mM phosphate–D_2O, pH 6.9 at 30 °C.

attachment of AF at the C8 position of G6. This directionality to the NOEs is also detected between the base protons and their own and 5′-flanking sugar H3′ protons and sugar H2′,2″ protons, enabling these sugar protons to be partially assigned in an analogous manner.

The sugar proton assignments can be independently verified from the coupling connectivities in the COSY, DQF-COSY, and HOHAHA two-dimensional spectra. An expanded magnitude COSY contour plot establishing coupling connectivities between the 4.2–6.4 ppm H1′ and H3′ region and the 1.8–3.8 ppm H2′,2″ region in the (AF)G 11-mer duplex at 30 °C is plotted in Figure 4A. A striking observation is the 1.41 ppm chemical shift difference between the H2′,2″ protons of (AF)G6 coupled with an inversion in the coupling patterns at this residue. These results establish that the 3.68 ppm H2′ proton of the (AF)G6 lesion site has undergone a large selective downfield shift in the (AF)G 11-mer duplex.

The adenosine H2 protons are readily identified by inversion–recovery experiments as a consequence of their long spin–lattice relaxation time values. Four of these adenosine H2 protons are in A·T pairs and have been assigned from the observed NOEs between the thymidine imino protons and the adenosine H2 protons. The remaining adenosine H2 proton is assigned to A17, which is opposite the (AF)G6 lesion site. The H2 proton of A17 broadens significantly on lowering of the temperature to 5 °C in contrast to the H2 protons of A3, A9, A15, and A19 which exhibit no pronounced changes in line width with decreasing temperature.

The base and sugar H1′, H2′,2″, and H3′ nonexchangeable proton chemical shifts in the (AF)G 11-mer duplex at 30 °C are listed in Table II. It should be noted that the H8 protons of G16 (6.95 ppm) and G18 (7.15 ppm) flanking the lesion site are shifted to high field relative to the H8 protons of the other guanosines (7.75–7.80 ppm) with the effect more pronounced for G16 than for G18 (see Table II and Figure 3B). Further, the H2 proton of A17 (8.00 ppm) at the lesion site is the most downfield of the adenosine H2 protons in the (AF)G 11-mer duplex (Table II).

Nonexchangeable Aminofluorene Protons. The aminofluorene protons of (AF)G6 can be subdivided into four classes on the basis of the observed NOEs to protons in the trinucleotide duplex segment centered about the (AF)G6·A17 lesion site in the (AF)G 11-mer duplex.

The first class of aminofluorene protons which are related by NOE and coupling connectivities consist of the geminal H9 protons and the H1 and H8 protons that flank them. The 8.00 ppm H2 proton of A17 exhibits a moderate NOE to the 7.19 ppm aminofluorene H1 proton (boxed peak, Figure 4B), weak NOEs to the 3.16 and 3.28 ppm geminal aminofluorene H9 protons (peaks A and B, Figure 5A), and no NOE to the 6.83 ppm aminofluorene H8 proton of (AF)G6 in the (AF)G 11-

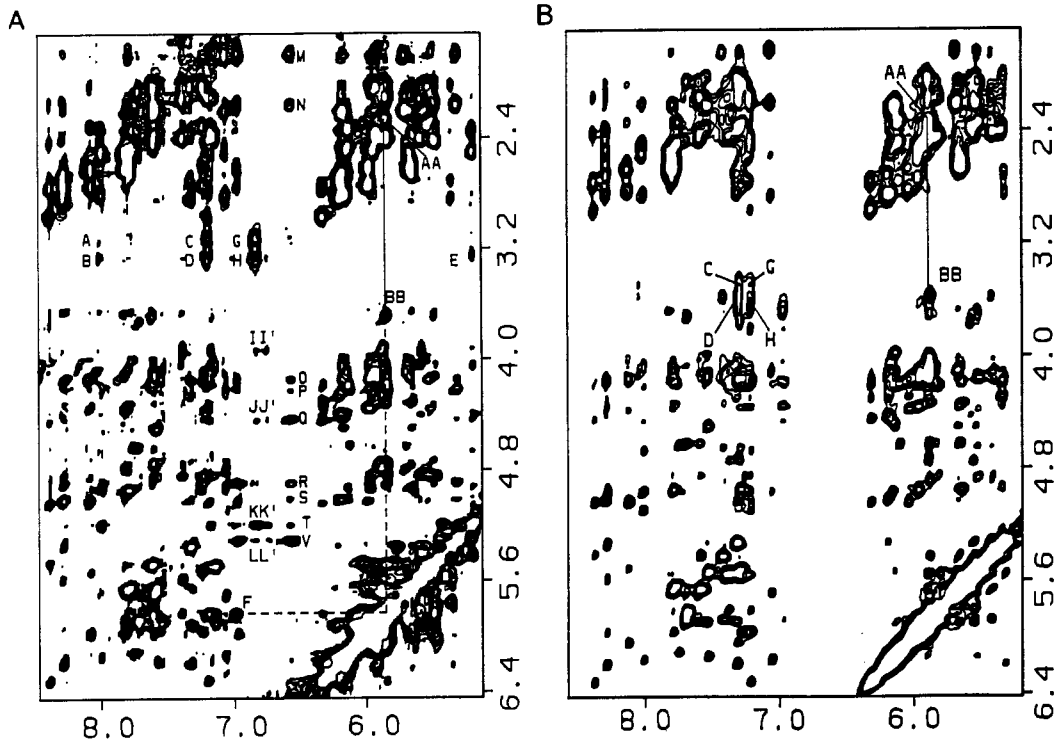

FIGURE 5: Phase-sensitive NOESY contour plots (mixing time 300 ms) of the (AF)G 11-mer duplex in 0.1 M NaCl–10 mM phosphate–D_2O, establishing distance connectivities between the 5.2–8.4 ppm and the 1.6–6.2 ppm regions. (A) pH 6.9 at 30 °C. (B) pH 5.9 at 20 °C. The labeled crosspeaks are assigned as follows: A/B, AF(H9,H9)–A17(H2); C/D, AF(H9,H9)–AF(H1); G/H, AF(H9,H9)–AF(H8); I/I′, AF(H5/H7,H8)–G18(H5′,5″); J/J′, AF(H5/H7,H8)–G18(H4′); K/K′, AF(H5/H7,H8)–G18(H1′); L/L′, AF(H5/H7,H8)–G16(H1′); M/N, AF(H5/H7,H6)–G16(H2′,H2″); O/P, AF(H5/H7,H6)–G16(H4′,H5′,H5″); Q, AF(H5/H7,H6)–G18(H4′); R, AF(H5/H7,H6)–G16(H3′); S, AF(H5/H7,H6)–A17(H3′); T, AF(H5/H7,H6)–G18(H1′); V, AF(H5/H7,H6)–G16(H1′); AA, G6(H1′)–G6(H2″); BB, G6(H1′)–G6(H2′); F, AF(H3/H4)–G6(H1′).

Table II: Nonexchangeable Proton Chemical Shifts in the (AF)G 11-mer in 0.1 M NaCl–10 mM Phosphate–D_2O, pH 6.9, 30 °C

	chemical shifts (ppm)						
base	H8	H6	H2	H5/CH_3	H1′	H2′,2″	H3′
C1		7.70		5.87	6.13		4.49
C2		7.58		5.67	5.46		4.84
A3	8.36		7.80		6.30	2.74, 2.96	5.03
T4		7.17		1.48	5.82	2.69, 2.83	4.84
C5		7.12		5.48	5.89	1.77, 1.77	4.93
(AF)G6					5.83	3.68, 2.27	4.92
C7		7.59		5.46	5.82		4.85
T8		7.36		1.55	5.57	2.11, 2.39	4.82
A9	8.27		7.55		6.17	2.70, 2.82	5.01
C10		7.30		5.33	5.90	2.02, 2.36	4.73
C11		7.56		5.63	6.15		4.50
G12	7.81				5.64		4.77
G13	7.78				5.95		4.94
T14		7.21		1.38	5.51		4.84
A15	8.05		7.39		5.96	2.62, 2.74	5.02
G16	6.95				5.29	1.78, 2.16	4.90
A17	8.25		8.00		6.15		5.01
G18	7.15				5.18	2.34, 2.50	4.68
A19	7.98		7.72		6.13	2.49, 2.80	4.92
T20		7.04		1.23	5.68	1.79, 2.20	4.80
G21	7.76				5.64		4.94
G22	7.74				6.11		4.62

mer duplex. These NOEs help align the minor groove edge of A17 and the geminal H9 proton containing aminofluorene edge of (AF)G6 at the lesion site.

The second class of aminofluorene protons consists of the 6.97 ppm resonance which exhibits NOEs to the sugar H1′ proton of (AF)G6 (peak F, Figure 5A) and is assigned to the aminofluorene H3 and H4 protons adjacent to the covalent linkage site. The sugar H1′ protons are located in the minor groove and confirm the alignment of aminofluorene in the minor groove of the (AF)G 11-mer duplex.

The third class of aminofluorene protons consists of the 6.74 ppm resonance (assigned to either H5 or H7) which along with the 6.83 ppm resonance (assigned above to H8) exhibits NOEs to the same minor groove sugar protons in the G16-A17-G18 segment on the partner strand (peaks I and I′, peaks J and J′, peaks K and K′, and peaks L and L′, Figure 5A).

The last class of aminofluorene protons are superpositioned at 6.56 ppm (assigned either to H5 and H6 or to H6 and H7) and also exhibit NOEs to minor groove sugar protons in the G16-A17-G18 segment (peaks M, N, O, P, Q, R, S, T, and V, Figure 5A). These NOEs establish that the aminofluorene ring of (AF)G6 furthest from the linkage site spans the minor groove and is aligned toward the G16-A17-G18 segment on the partner strand.

Backbone Phosphates. The proton-decoupled phosphorus spectrum of the (AF)G 11-mer duplex in D_2O buffer, pH 6.9 at 30 °C, is plotted in Figure 1C. The phosphorus resonances are dispersed over 0.9 ppm with several resonances shifted to low and high field of the −4.0 to −4.5 ppm spectral dispersion characteristic of unperturbed DNA helices. The three- and four-bond proton–phosphorus vicinal couplings permit correlation of the phosphorus resonances with the protons on the sugar rings in the O3′- and O5′-directions in nucleic acid duplexes (Pardi et al., 1983; Sklenar et al., 1986). A contour plot of the proton-detected proton–phosphorus heteronuclear COSY experiment on the (AF)G 11-mer in D_2O, pH 6.9 at 30 °C, is plotted in Figure B (supplementary material). Each phosphorus resonance exhibits crosspeaks to the H3′ proton (4.6–5.1 ppm) in the O3′-direction and to the H4′ and H5′,5″ protons (3.9–4.5 ppm) in the O5′-direction. Eighteen of the twenty possible crosspeaks between phosphorus and sugar H3′ protons can be resolved in the contour plot (Figure B). The overlap of the sugar H3′ assignments (Table II) prevents definitive assignments of the phosphorus resonances of the

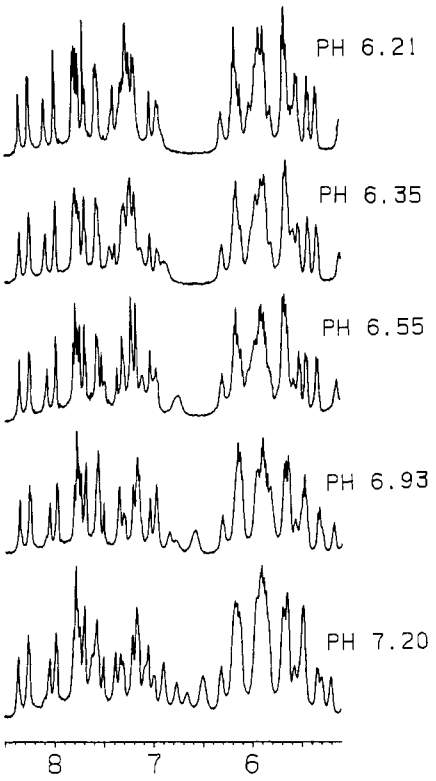

FIGURE 6: Proton NMR spectra (5.0–8.5 ppm) of the (AF)G 11-mer duplex in 0.1 M NaCl–10 mM phosphate–D_2O, 30 °C at pH 6.21, 6.35, 6.55, 6.93, and 7.20.

Table III: Upper-Bound Distance Constraints Centered about the [C5-(AF)G6-C7]·[G16-A17-G18] Segment Employed in Energy Minimizations of (AF)G 11-mer Conformation at Neutral pH

atom pair	upper-bound distance (Å)
A17(H2)–AF(H1)	3.0[a]
A17(H5′/5″)–AF(H6/7)	4.5[a]
G18(H4′)–AF(H6/7)	4.5[a]
G16(H2″)–AF(H6/7)	4.5[a]
G16(H1′)–AF(H6/7)	4.0[a]
G18(H1′)–AF(H8)	4.5[a]
G6(H1′)–AF(H3)	4.5[a]
G6(N3)–G6(H1′)	3.9[b]

[a] Lower bound is sum of van der Waals radii plus 0.2 Å. These constraints were derived from measured NOEs. Slashes, where present, indicate that NOEs could not distinguish the atoms separated by the slash. All possible combinations were individually tried in distance-constrained minimizations for trimers. The lowest energy trimers were computed for constrainted AF(H7) and A17(H5′). The AF(H6) and A17(H5″) constraint was therefore not employed in larger structures. Equation 2 was used to constrain these distances. [b] Derived from a model generated to best match the experimental data. A large downfield chemical shift for G6(H2′) shows that N3 of the *syn*-guanine is very close to its H2′. The G6(N3)–G6(H1′) constrained distance achieves this orientation. Equation 3 was used to constrain this distance.

(AF)G 11-mer duplex on the basis of the contour plot in Figure B.

NMR Distance Constraints. The crosspeaks corresponding to the NOEs between the base and their own sugar H1′ protons overlap for A9 and A17 at pH 6.9 (peaks labeled A9 and A17 in Figure 3). Earlier research has established that the intensities of the NOE between the bases and their own sugar H1′ protons for the syn-glycosidic torsion angle are comparable (interproton distance ~2.5 Å) while those for the anti-glycosidic torsion angle are weak (interproton distance ~3.7 Å) relative to the NOE between the H5 and H6 protons of cytidine (fixed distance of 2.45 Å) (Patel et al., 1982). Experimentally, the intensity of the NOE between the superpositioned H8 and H1′ protons of A9 and A17 is weaker than the NOE between the H5 and H6 protons of cytidine in the (AF)G 11-mer duplex, pH 6.9 and 30 °C, establishing that A17 adopts an anti-glycosidic torsion angle in the (AF)G 11-mer duplex. The 8.00 ppm H2 proton of A17 would be located in the minor groove for an anti orientation about the glycosidic bond.

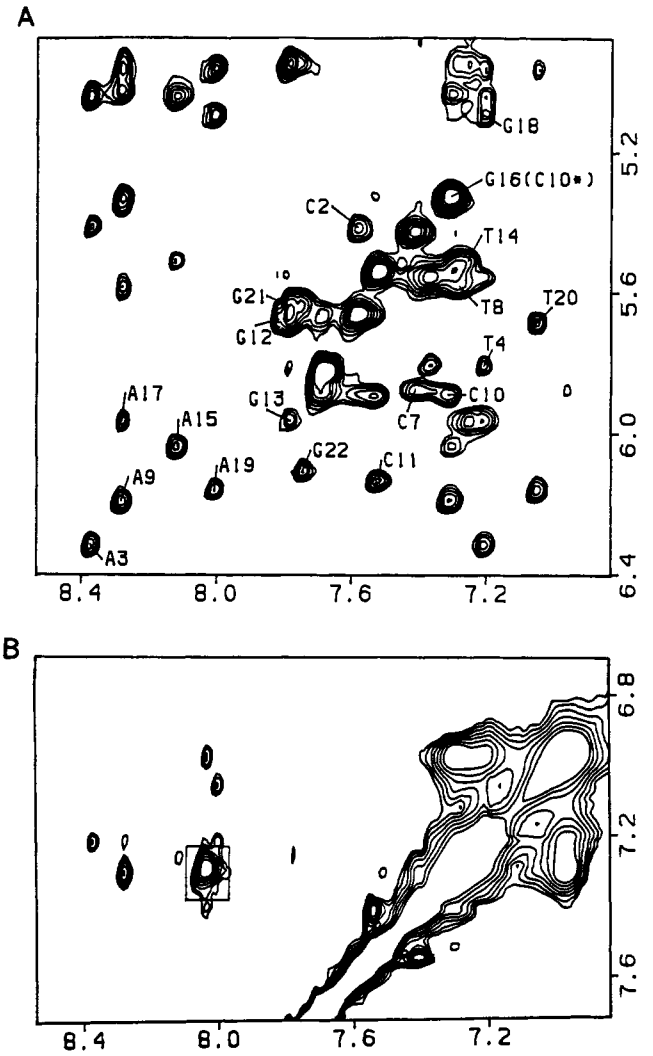

FIGURE 7: Expanded phase-senstive NOESY contour plots (mixing time 300 ms) of the (AF)G 11-mer duplex in 0.1 M NaCl–10 mM phosphate–D_2O, pH 5.9 at 20 °C. (A) Crosspeaks establishing distance connectivities between the base protons (6.8–8.4 ppm) and the sugar H1′ and cytidine H5 protons (5.0–6.4 ppm). The labeled crosspeaks correspond to NOEs between base protons and their own sugar H1′ protons. Note that crosspeaks labeled A9 and A17 are resolved in the contour plot. (B) Crosspeaks establishing distance connectivities between the 7.0–8.4 ppm and the 7.0–7.6 ppm regions.

The observed NOE between the 8.00 ppm H2 proton of A17 and the 7.19 ppm aminofluorene H1 proton at pH 6.9 (boxed peak, Figure 4B) establishes that the aminofluorene ring is located in the minor groove of the (AF)G 11-mer duplex at neutral pH. This can only occur if the (AF)G6 adopts a syn torsion angle about the glycosidic bond.

Further, the observed NOEs between the aminofluorene H5, H6, H7, and H8 protons at the (AF)G6 lesion site and the sugar protons of the G16-A17-G18 segment (Figure 5A) establish that the aromatic ring of aminofluorene furthest from the covalent linkage site interacts with sugars on the partner strand in the minor groove of the (AF)G 11-mer duplex at neutral pH.

The experimental set of NOE-based constraints between the aminofluorene ring protons and the nucleic acid protons in the

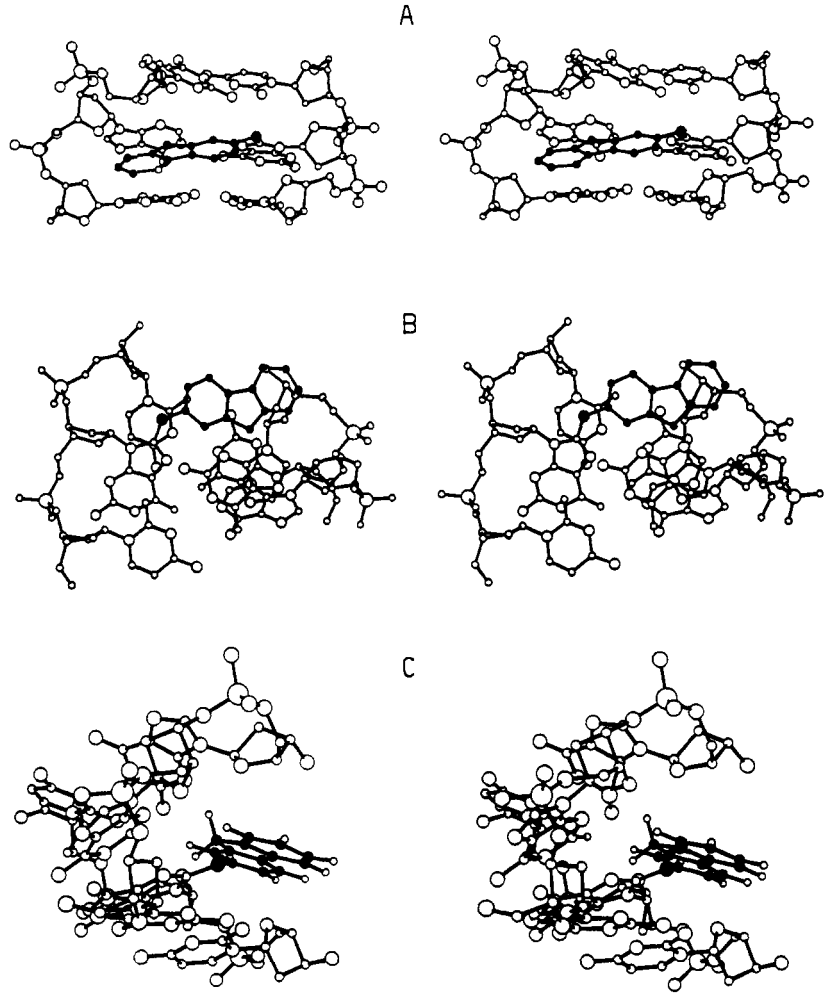

FIGURE 8: Three stereoviews of the [C5-(AF)G6-C7]·[G16-A17-G18] trinucleotide segment of the fully constrained energy minimized (AF)G 11-mer duplex at neutral pH. These stereoviews are prepared for use with a stereoviewer. Left and right images must be interchanged to view with crossed eyes. View A emphasizes the location of AF in the minor groove and the extension of the AF ring toward the sugar–phosphate backbone on the partner strand. View B shows the poor overlap between the bases in the C5-(AF)G6-C7 segment and the good overlap between bases in the G16-A17-G18 segment. View C emphasizes the interaction of AF with the walls of the minor groove. The (AF)G linkage torsion angles are $\alpha' = 208°$ and $\beta' = 317°$ (see Experimental Procedures for definition). Torsion angles that differ from those observed in the major B_I conformer of the B-DNA dodecanucleotide crystal (Drew et al., 1981; Dickerson, 1987) are as follows: χ(AF)G6 = 71°; P(G16) = 33°, ϵ(A17) = 281°, ζ(A17) = 145°, and β(G18) = 134°. Torsion angles of the trinucleotide segment are listed in Table V.

[C5-(AF)G6-C7]·[G16-A17-G18] segment of the (AF)G 11-mer duplex, pH 6.9, is defined by upper bounds in Table III.

(2) NMR Assignments and Constraints for (AF)G 11-mer at Acidic pH

A pH-dependent transition has been detected centered about the (AF)G6·A17 lesion site in the (AF)G 11-mer duplex. This section focuses on the conformational parameters for the [C5-(AF)G6-C7]·[G16-A17-G18] segment at acidic pH with the emphasis on a comparative study with the conformational parameters at neutral pH.

Exchangeable Protons. The imino proton spectra (9.0–15.0 ppm) of the (AF)G 11-mer duplex in H_2O buffer, 15 °C, at pH 5.12, 6.12 and 6.75 are plotted in Figure C (supplementary material). The imino proton of G16 shifts dramatically downfield on lowering the pH below neutrality while the effect is less pronounced for the imino proton of G18 (Figure C). By contrast, the chemical shift of the imino proton of (AF)G6 remains essentially unchanged between pH 5.12 and pH 6.75 in the (AF)G 11-mer duplex at 15 °C. Finally, no additional exchangeable proton resonances were detected between 9 and 11 ppm on lowering of the pH of the (AF)G 11-mer sample from pH 6.75 to pH 5.12 (Figure C).

Nonexchangeable Protons. The nonexchangeable proton spectra (5.0–8.5 ppm) of the (AF)G 11-mer duplex in D_2O buffer, 30 °C, between pH 6.21 and pH 7.20 are plotted in Figure 6. The nonexchangeable aminofluorene protons that resonate between 6.5 and 7.0 ppm in the (AF)G 11-mer duplex at pH 7.20 shift dramatically downfield as average resonances with some broadening on lowering of the pH in steps to pH 6.21. This can be most easily visualized in the 6.3–6.9 ppm spectral region where aminofluorene resonances are detected at pH 7.20 while this region is free of resonances at pH 6.21 in the (AF)G 11-mer duplex (Figure 6). The shifts are large since the 6.5 ppm aminofluorene resonance at pH 7.20 shifts downfield to 6.95 ppm at pH 6.21. The aminofluorene protons that undergo downfield shifts on lowering of the pH have been assigned to the H5, H6, H7, and H8 protons on the aminofluorene aromatic ring furthest from the covalent linkage site.

An expanded NOESY (300-ms mixing time) contour plot establishing distance connectivities between the base protons (6.9–8.4 ppm) and the sugar H1′ and cytidine H5 protons (5.1–6.4 ppm) of the (AF)G 11-mer duplex, pH 5.9 at 20 °C, is plotted in Figure 7A. The crosspeaks corresponding to NOEs between base protons and their own sugar H1′ protons are labeled in Figure 7A. It should be noted that the crosspeaks labeled A9 and A17 are superpositioned in the pH 6.9

contour plot (Figure 3) but are resolved in the pH 5.9 contour plot (Figure 7A). Further, the H8 proton of G16 shifts downfield from 6.95 ppm at pH 6.9 (Figure 3A) to 7.31 ppm at pH 5.9 (Figure 7A) while a much smaller perturbation is detected for the H8 proton of G18 which shifts downfield from 7.15 ppm at pH 6.9 (Figure 3A) to 7.20 ppm at pH 5.9 (Figure 7A).

A strong NOE is detected between the H2 proton of A17 and the H1 aminofluorene proton of (AF)G6 in the NOESY (300-ms mixing time) spectrum of the (AF)G 11-mer duplex in D_2O buffer, pH 5.9 (boxed peak, Figure 7B), similar to what was detected in the corresponding data at pH 6.9 (boxed peak, Figure 4B). The H2 proton of A17 shifts very slightly from 8.00 ppm at pH 6.9 to 8.03 ppm at pH 5.9 while the H1 aminofluorene proton of (AF)G6 shifts from 7.19 ppm at pH 6.9 to 7.29 ppm at pH 5.9.

A large chemical shift difference is observed between the H2′ and H2″ protons of (AF)G6 for the (AF)G 11-mer duplex at pH 5.9 (crosspeaks AA and BB, Figure 5B) similar to what was detected at pH 6.9 (crosspeaks AA and BB, Figure 5A). The H2′ proton of (AF)G6 resonates at 3.68 ppm at pH 6.9 and at 3.58 ppm at pH 5.9.

The geminal H9′,9″ aminofluorene protons resonate at ~3.2 ppm in the (AF)G 11-mer duplex at pH 6.9 (peaks C–H, Figure 5A) but shift downfield to ~3.6 ppm in the (AF)G 11-mer duplex at pH 5.9 (peaks C–H, Figure 5B).

A large set of NOE crosspeaks were detected between the H5, H6, H7, and H8 aminofluorene protons of (AF)G6 and the sugar protons of the G6-A17-G18 segment in the NOESY spectrum of the (AF)G 11-mer duplex at pH 6.9 (peaks I–V, Figure 5A). We have not detected the corresponding NOEs in the NOESY spectrum of the (AF)G 11-mer duplex at pH 5.9 (Figure 5B).

(3) Conformational Computations

Minimization Search Procedures. Conformation space searches (methodology outlined under Experimental Procedures) were guided by the experimental finding that the AF-modified guanosine is syn and its opposite adenosine is anti in the (AF)G 11-mer at neutral pH and acidic pH and that the overall structure is B-form DNA. In addition, the observation of a moderate-intensity NOE between the H1 aminofluorene proton of (AF)G6 and the H2 proton of A17 at both neutral pH (Figure 4B) and acidic pH (Figure 7B) suggested, from preliminary model building, that a short distance may exist between the O6 of (AF)G6 and the N1 of A17. A potential hydrogen bond could be generated between these atoms through protonation at the N1 position of A17, and this hydrogen bond was employed in the first stage of the conformational searches. Initially, the central trinucleotide [C5-(AF)G6-C7]·[G16-A17-G18] segment was investigated without distance constraints.

The conformational space about the torsion angles α' and β' defining the AF–guanosine linkage site (**2**) was explored in the AF-modified central trinucleotide segment as follows: the (C5-G6-C7)·(G16-A17-G18) segment without AF was first energy minimized from a B-DNA fiber diffraction conformation (Arnott et al., 1976) with the hydrogen-bond forcing function (eq 1) implemented to locate Watson–Crick base pairs at C5·G16 and C7·G18. For the central G6 (whose conformation was syn, $\chi = 60°$) and A17 bases which are opposite each other, the hydrogen-bonding function was employed to search for the hydrogen bond between the O6 of G6 and protonated N1 of A17. Energy minimizations were undertaken with this starting conformation for α', β' (AF)G6 linkage

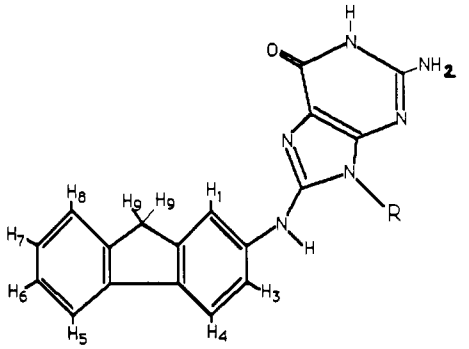

2

angles in one of the following 16 combinations: $\alpha' = 0, 90, 180, 270°$; $\beta' = 0, 90, 180, 270°$.

The lowest energy protonated trinucleotide found in the unconstrained searches had overall conformational features consistent with the NMR constraints: *syn*-guanosine with aminofluorene in the minor groove and in contact with the opposite strand and *anti*-adenosine. However, only three of eight NOE measured distances (Table III, items 2, 4, and 8) were below 4.5 Å, which represents the cutoff range for detectable NOE crosspeaks for the (AF)G 11-mer duplex at neutral pH. At this point distance constraints were employed in a subsequent series of minimizations, using the contraints and procedures given in Table III. A range of weights was employed until structures were achieved with distances within the target range. W_{HB} was retained in these trials. This structure designated the "constrained protonated trinucleotide conformation" serves as the starting model for the minimization studies of the neutral pH and acidic pH conformations presented below.

Neutral pH Energy Minimized Conformation. Several building strategies were employed to search for energy minimized (AF)G 11-mers that matched the neutral pH NMR data. The approach that yielded an unconstrained energy minimized (AF)G 11-mer duplex which satisfied the NMR distance constraints is the following: The B-form block consisting of the duplex residues 1–4 and 19–22 was preminimized. Next, the constrained protonated trinucleotide conformation (residues 5–7 and 16–18) was added, and the energy was minimized with all constraints. Then, one additional residue at a time was added in the B-form to generate the (AF)G 11-mer duplex, and the energy was minimized with all constraints at each step. The penultimate stage of the refinement involved removal of the proton at N1 of A17 along with its hydrogen-bond forcing function. Lastly, all other W_{HB}, and then W_N and W_S, were released in two subsequent minimizations, yielding fully unconstrained structures that were energy minima. The fully unconstrained conformations differed by small movements from the final constrained structures but remained within range of the experimental observations.

Three views of the central modified trinucleotide [C5-(AF)G6-C7]·[G16-A17-G18] segment of the energy minimized (AF)G 11-mer duplex at neutral pH are shown in stereo in Figure 8. The experimental distance constraints listed in Table III were satisfied in the neutral pH conformation of the (AF)G 11-mer duplex and are also listed in Table IV. The backbone torsion angles for the [C5-(AF)G6-C7]·[G16-A17-G18] segment of the neutral pH conformation of the (AF)G 11-mer duplex are listed in Table V.

The alignment of the aminofluorene ring of (AF)G6 relative to the two strands is emphasized in Figure 8A while the in-

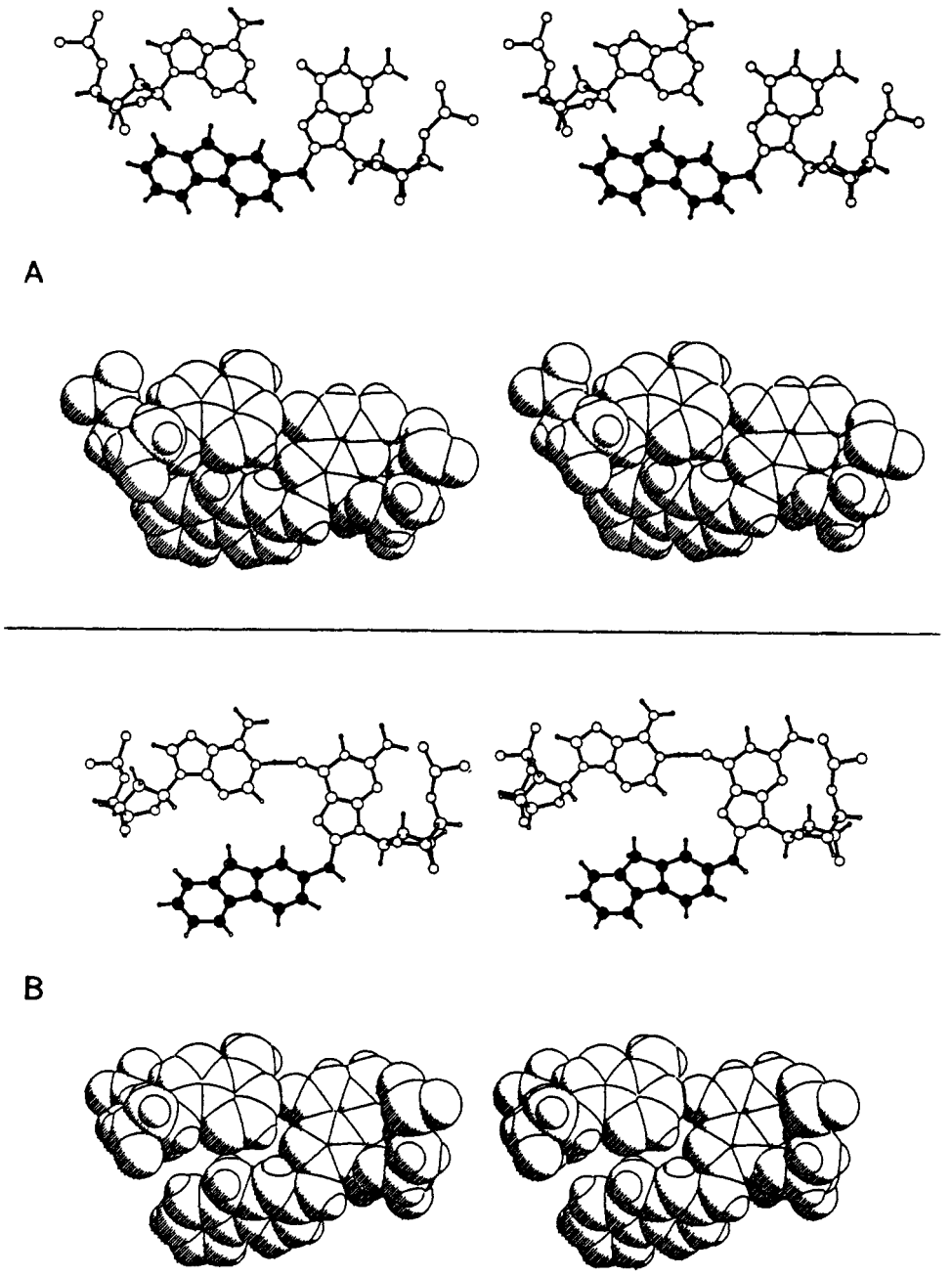

FIGURE 9: (A) A ball and stick (top) and space-filling (bottom) stereo pair of the pairing alignment at the (AF)G6[syn]·A17[anti] lesion site in the fully unconstrained energy minimized (AF)G 11-mer duplex at neutral pH. (B) A ball and stick (top) and space-filling (bottom) stereo pair of the pairing alignment at the protonated (AF)G6[syn]·A17[anti] lesion site in the energy minimized [C5-(AF)G6-C7]·[G16-A17-G18] segment of the (AF)G 11-mer duplex at acidic pH.

Table IV: Interproton Distances in the Energy Minimized Neutral pH Conformation of the (AF)G 11-mer Duplex

atom pair	distance (Å)
A17(H2)–AF(H1)	2.26
A17(H5′)–AF(H7)	4.31
G18(H4′)–AF(H7)	3.84
G16(H2″)–AF(H7)	4.18
G16(H1′)–AF(H7)	4.71
G18(H1′)–AF(H8)	4.86
G6(H1′)–AF(H3)	4.02

Table V: Backbone Torsion Angles for the [C5-(AF)G6-C7]·[G16-A17-G18] Segment in the Energy Minimized Neutral pH Conformation of (AF)G 11-mer

	α	β	γ	P	χ	ϵ	ζ
C5	305	182	52	161	232	193	223
(AF)G6	304	178	50	140	71	182	253
C7	304	171	54	155	244	179	257
G16	283	182	42	33	221	210	283
A17	299	169	62	168	244	281	145
G18	282	134	54	150	235	182	247

sertion of the aminofluorene ring within the walls of the minor groove is emphasized in Figure 8C. The stacking patterns in the modified C5-(AF)G6-C7 segment and the unmodified G16-A17-G18 segment are emphasized in Figure 8B.

The alignment of (AF)G6[syn] and A17[anti] at the (AF)G6·A17 pair in the energy minimized (AF)G 11-mer at neutral pH is shown in a ball and stick stereo drawing in Figure 9A (top) and a space-filling stereo drawing in Figure 9A (bottom).

Acidic pH Energy Minimized Conformation. The NOE experimental data establish an (AF)G6[syn]·A17[anti] alignment and a short interproton distance between the am-

inofluorene H1 proton of (AF)G6 and the H2 proton of A17 for the (AF)G 11-mer duplex at acidic pH (Figure 7B). By contrast, the other distance constraints defined for the neutral pH conformation (Figure 5A, Table III) are either longer than the 4.5-Å cutoff distance or cannot be estimated due to potential spectral overlap of crosspeaks in the NOESY spectrum for the acidic pH conformation (Figure 5B). The constrained protonated trinucleotide conformation was minimized with all distance constraints lifted except that between the H1 of (AF)G6 and the H2 of A17 while retaining the hydrogen-bond forcing function ($W_{HB} = 50$) between the O6 of (AF)G6 and the N1 of A17 at the (AF)G6[syn]·A17[anti] modification site.

The alignment of the (AF)G[syn] and A17[anti] at the (AF)G6·A17 pair in this energy minimized trinucleotide segment at acidic pH is shown in the ball and stick stereo drawing in Figure 9B (top) and a space-filling stereo drawing in Figure 9B (bottom).

Discussion

Our initial NMR studies focused on the (AF)G adduct positioned opposite C in the center of a series of DNA oligomer duplexes. The exchangeable and nonexchangeable proton NMR spectra of such sequences gave a combination of narrow and broad lines indicative of conformational heterogeneity precluding any attempt at a detailed two-dimensional proton NMR study of the aminofluorene adduct of guanosine positioned opposite cytidine at the duplex level in solution.

We have been far more successful in our NMR studies of the (AF)G adduct positioned opposite A in the center of the (AF)G 11-mer duplex (**1**). The resonances are sufficiently narrow at a given pH value to assign the exchangeable and nonexchangeable base protons, the majority of the sugar protons and a partial assignment of the aminofluorene protons in two-dimensional data sets of the (AF)G 11-mer duplex. The observed NOEs can then be translated into qualitative distance constraints to define the conformation of the trinucleotide segment centered about the (AF)G6·A17 modification site.

The NMR chemical shift parameters establish a pH-dependent conformational transition for the (AF)G 11-mer duplex, and hence, the discussion will address first the structural features of the neutral pH conformation followed by the acidic pH conformation. A large number of experimental distance constraints are available between the aminofluorene and the nucleic acid for the neutral pH conformation relative to the acidic pH conformation. This has permitted a more precise definition of the alignment of the (AF)G6·A17 pairing and the orientation of the aminofluorene ring at the modificate site in the neutral pH conformation.

(1) Neutral pH Conformation

The aminofluorene nonexchangeable ring protons readily monitor the pH-dependent structural transition in the (AF)G 11-mer as has been demonstrated in Figure 6 in the pH range 6.21 to 7.20. The transition is not complete on the basic pH side by pH 7.20, but concerns regarding the stability of the adduct to alkaline conditions prevented a further increase of pH. The term neutral pH conformation represents the predominant structure of the (AF)G 11-mer duplex generated at pH values somewhat higher than neutrality.

Global Structure Features. Several conclusions regarding the global structural features of the helix can be deduced from the observed NOE parameters of the exchangeable and nonexchangeable protons of the (AF)G 11-mer duplex. The observed NOEs between thymidine imino and adenosine H2 protons (Figure 2B) establish Watson–Crick A·T pairing while the observed NOEs between guanosine imino and cytidine amino protons (Figure 2B) establish Watson–Crick G·C pairing at all positions along the helix save the (AF)G6·A17 modification site in the (AF)G 11-mer duplex.

The observed directionality of the NOEs between the base (purine H8 or pyrimidine H6) protons and their own and 5′-flanking sugar H1′ protons establishes that the (AF)G 11-mer helix is right-handed and regular between the positions C1 to C5 and C7 to C11 on the modified strand (Figure 3A) and G12 to G22 on the unmodified strand (Figure 3B). Since (AF)G6 lacks an H8 proton, this approach does not define the helix handedness at the modification site.

The base to its own sugar H1′ NOE crosspeaks for all unmodified bases are much weaker than the strong NOE between the H6 and H5 protons of cytidine (Figure 3), consistent with all unmodified bases adopting an anti-glycosidic torsion angle in the (AF)G 11-mer duplex. The absence of an H8 proton for (AF)G6 does not permit an estimate of the glycosidic torsion angle range at the modification site on the basis of the above approach.

(AF)G6 Modification Site. The alignment of (AF)G6 and A17 is defined by the moderate-intensity NOE detected between the aminofluorene H1 proton of (AF)G6 and the H2 proton of A17 in the (AF)G 11-mer duplex at pH 6.9 (boxed peak, Figure 4B). This distance connectivity simultaneously defines the glycosidic torsion angle range for (AF)G6, differentiates between positioning the aminofluorene between the minor and major groove, and defines which edge of the aminofluorene chromophore is directed toward solvent. Since A17 exhibits an anti-glycosidic torsion angle, its H2 proton must be directed into the minor groove of the (AF)G 11-mer duplex. The observed NOE between the (AF)G6 H1 proton and the A17 H2 proton mandates that the aminofluorene be positioned in the minor groove which can only occur if (AF)G6 adopts a syn-glycosidic torsion angle. Finally, the observed NOE establishes that the aminofluorene edge bearing the H1 and geminal H9 protons be directed toward the interior of the helix while the edge bearing the H4 and H5 protons be directed toward solvent.

The imino proton and amino protons of (AF)G6 in a syn orientation are directed toward the major groove and are not hydrogen bonded to acceptor groups. This is consistent with the 10.98 ppm upfield chemical shift of the (AF)G6 imino proton (Figure 1A) and its rapid exchange characteristics as reflected in its strong exchange crosspeak with solvent H_2O (peak W, Figure 2B). The amino protons of (AF)G6 exhibit an average chemical shift at 6.4 ppm (peak T, Figure 2B) originating in rapid rotation around the C–NH_2 bond and consistent with absence of their participation in hydrogen-bond formation.

The energy minimized neutral pH conformation of the (AF)G 11-mer highlights these features as can be observed in the stereoviews of the (AF)G6(syn)·A17(anti) alignment at neutral pH (Figure 9A).

Aminofluorene Ring. The unambiguous positioning of the aminofluorene ring in the minor groove for the (AF)G6·A17 pair in the (AF)G 11-mer rules out models in which the aminofluorene ring stacks into the helix. Indeed, the aminofluorene ring positioned in the minor groove does not overlap with the aromatic rings of the flanking C5·G18 and C7·G16 base pairs in the energy minimized neutral pH structure of the (AF)G 11-mer duplex (Figure 8B).

The observed NOEs between the aminofluorene ring H5, H6, H7, and H8 protons which are furthest from the covalent linkage site and specific minor groove sugar protons on the

G16-A17-G18 segment (Figure 5A) establish that the aminofluorene ring spans the groove and interacts with the partner strand. This condition is satisfied in the energy minimized conformation of the (AF)G 11-mer as visualized in the stereo pair in Figure 8A.

The relative alignment of the aminofluorene ring and its covalently linked guanosine ring is governed by the two torsion angles (α' and β') of the intervening bonds. The energy minimized conformation is defined by α', β' values of 208°, 317° which position the aminofluorene ring with its H1 proton and geminal H9 proton edge directed toward the base pair edges in the minor groove. In fact, the aminofluorene ring is sandwiched between the walls of the minor groove of the helix as shown in the stereo pair in Figure 8C. This feature of a covalent ligand–DNA oligomer adduct has been observed earlier in the netropsin–DNA oligomer complex (Patel, 1982; Kopka et al., 1985) where the noncovalently bound antibiotic is also sandwiched between the walls of the minor groove.

The H2′ proton of (AF)G6 is dramatically shifted downfield in the (AF)G 11-mer duplex (Figure 4A). Such a downfield shift could be explained if the H2′ proton but not the H2″ proton of (AF)G6 was in the plane of the G6 ring and selectively experiences strong in-plane ring current contributions.

[C5-(AF)G6-C7]·[G16-A17-G18] Segment. The structural integrity of the trinucleotide segment centered about the (AF)G6·A17 modification site is of considerable interest. By switching to a syn-glycosidic torsion angle at (AF)G6, the bulky aminofluorene ligand can be positioned in the minor groove, resulting in formation of an (AF)G6[syn]·A17[anti] pair without major disruption of the helix.

The C5·G18 and C7·G16 base pairs are intact on either side of the (AF)G6·A17 modification site since the G18 and G16 imino protons can be detected in the exchangeable proton spectrum of the (AF)G 11-mer duplex (Figure 1A). The G18 imino proton is narrower than the G16 imino proton (Figure 1A), indicative of greater stability of the C5·G18 pair relative to the C7·G16 pair in the (AF)G 11-mer duplex.

The energy minimized neutral pH conformation of the (AF)G 11-mer exhibits distinct stacking patterns for the trinucleotide segments on the modified and unmodified strands (Figure 8B). Thus, there is minimal stacking between C5, (AF)G6, and C7 on the modified strand while there is strong overlap between the G16, A17, and G18 on the unmodified strand (Figure 8B). The observed strong stacking in the G16-A17-G18 segment may explain the unusually large upfield shifts of G16 (6.95 ppm) and G18 (7.15 ppm) in the (AF)G 11-mer duplex (Table II).

Torsion Angles. All torsion angles in the energy minimized conformation of the (AF)G 11-mer duplex were within the range of average values observed in the B-DNA dodecanucleotide crystal structure (Drew et al., 1981) except for those given in the caption in Figure 8 and underlined in Table V. The guanosine base is syn at the (AF)G6 modification site. The sugar ring pucker of G16 is C3′-endo on the partner strand. The backbone conformation of A17 has changed from the more common B_I conformation (ϵ, ζ = t, g$^-$) present in the rest of the structure to the B_{II} conformation (ϵ, ζ = g$^-$, t). These two alternate B-DNA conformers have been observed to coexist in a number of crystal structures (Dickerson, 1987) and appear to be readily interconvertible by changes in environmental conditions. The crystal data suggest that the predominant B_I state is only slightly lower in energy than the B_{II} state, with the modest energy barrier between them surmountable by forces whose magnitude is comparable to crystal packing forces (Dickerson et al., 1987). The B_I to B_{II} transition at A17 results, in part, in a small displacement of the A17 base toward the major groove in the neutral pH conformation of the (AF)G 11-mer duplex. As a consequence, the aminofluorene ring of (AF)G6 is readily accommodated in the minor groove and maximizes hydrophobic interactions associated with its extension toward the partner strand.

(2) Acidic pH Conformation

The NMR chemical shift and NOE parameters for the acidic pH conformation of the (AF)G 11-mer duplex exhibit both similarities and differences from the corresponding parameters for the neutral pH conformation.

The short interproton distance between the aminofluorene H1 proton of (AF)G6 and the H2 proton of A17 (boxed NOE crosspeak, Figure 7B) establishes that the (AF)G6[syn]·A17[anti] alignment and positioning of the aminofluorene ring in the minor groove are retained for (AF)G 11-mer at acidic pH.

The observed pH dependence could reflect formation of a protonated (AF)G6[syn]·A17[anti] pair at low pH through protonation of the N1 of adenosine and stabilized by two hydrogen bonds between the acceptor O6 carbonyl and N7 of *syn*-guanosine with the donor protonated N1 imino and N6 amino of protonated adenosine as has been established for the protonated G(syn)·A(anti) mismatch pair at low pH (Gao & Patel, 1988). This appears unlikely in the present structure since we do not detect the characteristic 10 ppm resonance of the hydrogen-bonded amino proton of protonated adenosine in the (AF)G 11-mer duplex at values as low as pH 5.12 (Figure C) as was detected for the protonated G(syn)·A(anti) mismatch containing duplex at low pH (Gao & Patel, 1988). Therefore, a single hydrogen bond was proposed linking the N1 of protonated A17 and O6 of (AF)G6, and this contact was retained during minimization runs on the acidic pH conformation.

The alignment of the (AF)G6[syn]·A17[anti] pair in the acidic pH conformation (Figure 9B) can be compared with the corresponding alignment in the neutral pH conformation (Figure 9A) by superpositioning the two structures as shown in Figure D (supplementary material). A major difference in the alignments is that the contacts between the aromatic ring of aminofluorene furthest from the linkage site and the G16-A17-G18 segment on the partner strand in the neutral pH conformation are lengthened significantly in the acidic pH conformation. This would account for the absence of NOEs between the H5, H6, H7, and H8 aminofluorene protons and the sugar protons of G16-A17-G18 segment in the acidic pH conformation. The associated movements of the aminofluorene ring further away from the helix axis in the acidic pH conformation may account for the downfield shift of the aminofluorene H5, H6, H7, and H8 protons on lowering of the pH from 7.20 to 6.21 (Figure 6).

Thus, our studies define the pH-dependent conformational transition in the (AF)G 11-mer duplex as a pivotal movement of (AF)G6[syn] relative to A17[anti] (Figure D) driven, in part, by formation of a single hydrogen bond under acidic conditions.

SUMMARY

The observed (AF)G6[syn]·A17[anti] alignment which results in positioning of the aminofluorene ring in the minor groove at the modification site differs from all previous structural models for the conformation of (AF)G in DNA helices. Our studies establish an interplay between hydrophobic interactions and hydrogen-bonding contributions to the stabilization at the modification site.

The neutral pH conformation is stabilized by hydrophobic interactions between the aminofluorene ring and the walls of the minor groove. This is facilitated, in part, by the B_I to B_{II} conformational transition at the A17 residue and a C3′-endo sugar pucker at the G18 residue and results in a small displacement of A17 toward the major groove. This relative positioning minimizes the total solvent-exposed surface of aminofluorene and A17 at the modification site. The neutral pH conformation of the (AF)G 11-mer is an unconstrained energy minimum which agrees with the NMR distance constraints and probably represents a dynamic family of related structures with similar conformational properties which maximize the hydrophobic interactions at the modification site.

The acidic pH conformation is stabilized, in part, by a single hydrogen bond proposed to form between the O6 of (AF)G6 and the N1 of A17 while retaining (AF)G6[syn]·A17[anti] alignment. The aminofluorene ring pivots away from the helix axis at acidic pH and breaks the contacts observed with the partner strand in the neutral pH conformation.

The covalently bound aminofluorene (AF) can be substituted by (acetylamino)fluorene (AAF) in the neutral pH conformation of the (AF)G 11-mer since there are no steric constraints to substitution of the NH functionality by the $NCOCH_3$ functionality. However, the proton NMR spectra of the (AAF)G 11-mer in which (AAF)G6 was positioned opposite A17 were a mixture of narrow and broad resonances, precluding attempts at detailed two-dimensional NMR studies.

It is interesting that in bacterial (Bichara & Fuchs, 1985; Gupta et al., 1988) as well as in mammalian systems (Carothers et al., 1989) the (AF)G adduct induces predominantly a G·C → T·A transversion. The mechanism that could result in this high degree of mutational specificity is the incorporation of A opposite the (AF)G in DNA during replication. Thus, this study supports the idea of the correlation between the conformational aspects of carcinogen-modified bases and mutational spectra.

The present study emphasizes the importance of coupling NMR-based distance constraints and energy minimization computations to define novel insights into the conformation of covalent carcinogen–DNA oligomer adducts in solution.

Acknowledgments

S.B. thanks Prof. Robert Shapiro, Chemistry Department, New York University, for many valuable discussions.

Supplementary Material Available

Table of partial charges of N^1-protonated adenosine (Table A) and figures showing the phase-sensitive NOESY contour plot of the (AF)G 11-mer duplex in H_2O (Figure A), the contour plot of the proton-detected proton–phosphorus heteronuclear COSY experiment on the (AF)G 11-mer duplex (Figure B), the exchangeable proton NMR spectra of the (AF)G 11-mer duplex as a function of pH (Figure C), and a stereo pair of the neutral pH and the acidic pH energy minimized conformations of the (AF)G[syn]·A17[anti] alignment in which the A17 are superpositioned on each other (Figure D) (6 pages). Ordering information is given on any current masthead page.

References

Altona, C., & Sundaralingam, M. (1972) *J. Am. Chem. Soc. 94*, 8205–8212.

Arnott, S., Campbell, P., & Chandrasekharan, R. (1976) in *Handbook of Biochemistry and Molecular Biology* (Fasman, G., Ed.) pp 411–422, CRC Press, Cleveland, OH.

Basu, A. K., & Essigmann, J. M. (1988) *Chem. Res. Toxicol. 1*, 1–18.

Beland, F., Dooley, K., & Jackson, C. (1982) *Cancer Res. 42*, 1348–1354.

Bichara, M., & Fuchs, R. P. (1985) *J. Mol. Biol. 183*, 341–351.

Broyde, S., & Hingerty, B. (1983) *Biopolymers 22*, 2423–2441.

Broyde, S., & Hingerty, B. (1987) *Nucleic Acids Res. 15*, 6539–6552.

Carothers, A. M., Steigerwalt, R. W., Urlaub, G., Chasin, L., & Grunberger, D. (1989) *J. Mol. Biol.* (in press).

Dickerson, R. (1987) in *Unusual DNA Structures* (Wells, R., & Harvey, S., Eds.) Spring-Verlag, New York.

Dickerson, R. E., Goodsell, D. S., Kopka, M. L., & Pjura, P. E. (1987) *J. Biomol. Struct. Dyn. 5*, 557–580.

Drew, H., Wing, R., Takano, T., Broka, C., Tanaka, S., Itakura, K., & Dickerson, R. (1981) *Proc. Natl. Acad. Sci. U.S.A. 78*, 2179–2183.

Evans, F. E., & Levine, R. A. (1987) *Biopolymers 26*, 1035–1046.

Evans, F. E., & Levine, R. A. (1988) *Biochemistry 27*, 3046–3055.

Evans, F. E., Miller, D., & Beland, F. (1980) *Carcinogenesis 1*, 955–959.

Fuchs, R. P., & Duane, M. (1972) *Biochemistry 11*, 2659–2666.

Gao, X., & Patel, D. J. (1988) *J. Am. Chem. Soc. 110*, 5178–5182.

Grunberger, D., Nelson, J., Cantor, C., & Weinstein, I. (1970) *Proc. Natl. Acad. Sci. U.S.A. 66*, 488–494.

Gupta, P. K., Lee, M. S., & King, C. M. (1988) *Carcinogenesis 9*, 1337–1345.

Hare, D. R., Wemmer, D. E., Chou, S. H., Drobny, G., & Reid, B. R. (1983) *J. Mol. Biol. 171*, 319–336.

Hingerty, B. E., & Broyde, S. (1982) *Biochemistry 21*, 3243–3252.

Hingerty, B. E., & Broyde, S. (1986) *J. Biomol. Struct. Dyn. 4*, 365–372.

Hingerty, B. E., Figueroa, S., Hayden, T., & Broyde, S. (1989) *Biopolymers* (in press).

Hunter, W., Brown, T., & Kennard, O. (1986) *J. Biomol. Struct. Dyn. 4*, 173–191.

Irving, C. (1966) *Cancer Res. 26*, 1390–1396.

Irving, C., & Veazey, R. (1969) *Cancer Res. 29*, 1799–1804.

Johnson, D. L., Reid, T. M., Lee, M. S., King, C. M., & Romano, L. J. (1986) *Biochemistry 25*, 449–456.

Kopka, M. L., Yoon, C., Goodsell, D., Pjura, P., & Dickerson, R. E. (1985) *J. Mol. Biol. 183*, 553–563.

Kriek, E. (1969) *Chem.-Biol. Interact. 1*, 3–17.

Kriek, E., & Spelt, C. (1979) *Cancer Lett. 7*, 147–154.

Krugh, T. R., Sanford, D. G., Walker, G. T., & Huang, G. (1986) *Pontif. Acad. Sci. 70*, 157–168.

Leng, M., Ptak, M., & Rio, P. (1980) *Biochem. Biophys. Res. Commun. 96*, 1095–1102.

Lipkowitz, K., Chevalier, T., Widdifield, G., & Beland, F. (1982) *Chem.-Biol. Interact. 40*, 57–76.

Live, D., Davis, D. G., Agosta, W. C., & Cowburn, D. (1984) *J. Am. Chem. Soc. 106*, 1939.

Michaels, M. L., Johnson, D. L., Reid, T. M., King, C. M., & Romano, L. J. (1987) *J. Biol. Chem. 262*, 14648–14654.

Mitchell, N., & Stohrer, G. (1986) *J. Mol. Biol. 191*, 177–180.

Neidle, S., Kurodo, R., Broyde, S., Hingerty, B. E., Levine, R. A., Miller, D. W., & Evans, F. E. (1984) *Nucleic Acids Res. 12*, 8219–8233.

O'Connor, D., & Stohrer, G. (1985) *Proc. Natl. Acad. Sci. U.S.A. 82*, 2325-2329.
Olson, W. (1978) *Biopolymers 17*, 1015-1040.
Ornstein, R., & Rein, R. (1979) *Biopolymers 18*, 1277-1291.
Pardi, A., Walker, R., Rapoport, H., Wider, G., & Wuthrich, K. (1983) *J. Am. Chem. Soc. 105*, 1652-1653.
Patel, D. J. (1982) *Proc. Natl. Acad. Sci. U.S.A. 79*, 6424-6428.
Patel, D. J., Kozlowski, S. A., Nordheim, A., & Rich, A. (1982) *Proc. Natl. Acad. Sci. U.S.A. 79*, 1413-1417.
Poirier, M., True, B., & Laishes, B. (1982) *Cancer Res. 42*, 1317-1321.
Prive, G., Heinemann, U., Chandrasegaran, S., Kan, L., Kopka, M., & Dickerson, R. (1987) *Science 238*, 498-504.
Rio, P., Malfoy, B., Sage, E., & Leng, M. (1983) *Environ. Health Perspect. 49*, 117-123.
Rubin, J., Brennan, T., & Sundaralingam, M. (1972) *Biochemistry 11*, 3112-3128.
Sage, E., Spodheim-Maurizot, M., Rio, P., Leng, M., & Fuchs, R. P. (1979) *FEBS Lett. 108*, 66-68.
Sanford, D. G., & Krugh, T. R. (1985) *Nucleic Acids Res. 13*, 5907-5917.
Santella, R., Kriek, E., & Grunberger, D. (1980) *Carcinogenesis 1*, 897-902.
Sharma, M., & Box, H. C. (1985) *Chem.-Biol. Interact. 56*, 73-88.
Singer, B., & Grunberger, D. (1983) *Molecular Biology of Mutagens and Carcinogens*, Plenum, New York.
Sklenar, V., & Bax, A. (1987) *J. Am. Chem. Soc. 109*, 7525.
Sklenar, V., Miyashiro, H., Zon, G., Miles, H. T., & Bax, A. (1986) *FEBS Lett. 208*, 94-98.
Srinivasan, A. R., & Olson, W. (1980) *Fed. Proc., Fed. Am. Soc. Exp. Biol. 39*, 2199.
States, D. J., Haberkorn, R. A., & Reuben, D. J. (1982) *J. Magn. Reson. 48*, 286-292.
Stohrer, G., Osband, J. A., & Alvarado-Urbina, G. (1983) *Nucleic Acids Res. 11*, 5093-5102.
van Houte, L. P. A., Bokma, J. T., Lutgerink, J. T., Westra, J. G., Retel, J., van Grondelle, R., & Blok, J. (1987a) *Carcinogenesis 8*, 759-766.
van Houte, L. P. A., Westra, J. G., Retel, J., van Grondelle, R., & Blok, J. (1987b) *Carcinogenesis 9*, 1017-1027.

Evidence for a Precursor of the High-Affinity Metastasis-Associated Murine Laminin Receptor†

C. N. Rao,‡ Vincent Castronovo, M. Christine Schmitt, Ulla M. Wewer,§ Anne P. Claysmith, Lance A. Liotta, and Mark E. Sobel*

Laboratory of Pathology, National Cancer Institute, Bethesda, Maryland 20892

Received March 30, 1989; Revised Manuscript Received May 25, 1989

ABSTRACT: The high-affinity cellular receptor for the basement membrane component laminin is differentially expressed during tumor invasion and metastasis. A cDNA clone encoding the murine laminin receptor was isolated and identified on the basis of sequence homology to the human laminin receptor [Wewer et al. (1986) *Proc. Natl. Acad. Sci. U.S.A. 83*, 7137-7141]. Primer extension experiments demonstrated that the clone contained the complete 5′ sequence of the murine laminin receptor mRNA. RNA blot data demonstrated a single-sized laminin receptor mRNA, approximately 1400 bases long, in human, mouse, and rat. The nascent laminin receptor predicted from the cDNA sequence is 295 amino acids long, with a molecular weight of 33 000, and contains one intradisulfide bridge, a short putative transmembrane domain, and an extracellular carboxy-terminal region which has abundant glutamic acid residues and multiple repeat sequences. The precursor of the laminin receptor is apparently smaller than the 67-kilodalton protein isolated from tissue. The apparent molecular weight on SDS-polyacrylamide gels of the rabbit reticulocyte cell-free translation product of selectively hybridized laminin receptor mRNA is 37 000. Antisera to three different domains of the cDNA-predicted receptor were used to study the relationship between the 37- and 67-kilodalton polypeptides. Antisera to cDNA-deduced synthetic peptides of the receptor immunoprecipitated a 37-kilodalton band both from cell-free translation products and from pulse-labeled cell extracts. On immunoblots of cell extracts, one antisynthetic peptide antiserum recognized only the 67-kilodalton receptor, while another antiserum identified both 37- and 67-kilodalton polypeptides, suggesting a precursor-product relationship between the two polypeptides.

Extracellular matrix molecules, notably laminin and fibronectin, play a significant role in important cellular events such as adhesion, morphology, spreading, migration, differentiation, tumor cell metastasis, and neurite outgrowth (Liotta et al., 1986, 1987; Ruoslahti, 1988). Studies on cell surface proteins which specifically interact with extracellular matrix molecules have identified specific receptors for these molecules and suggest that invasive and metastatic tumor cells have enhanced abilities to bind to the extracellular matrix (Liotta et al., 1986; Ruoslahti, 1988; Terranova et al., 1983; McCarthy et al., 1988; Humphries et al., 1986). Tumor cells must attach and interact with the basement membrane at several steps

† The nucleic acid sequence in this paper has been submitted to GenBank under Accession Number J02870.

* Address correspondence to this author at the Laboratory of Pathology, NCI, Building 10, Room 2A33, Bethesda, MD 20892.
‡ Present address: Connective Tissue Research Institute, University of Pennsylvania, 3624 Market St., Philadelphia, PA 19104.
§ Present address: University Institute of Pathological Anatomy, Frederik V's Vej 11, DK-2100 Copenhagen, Denmark.